ELSEVIER

Materials Characterization 58 (2007) 509–518

MATERIALS CHARACTERIZATION

TEM microstructural characterization of melt-spun aged Al–6Si–3Cu–*x*Mg alloys

Ismeli Alfonso López [a,*], Cuauhtémoc Maldonado Zepeda [a], José Gonzalo González Reyes [b], Ariosto Medina Flores [a], Juan Serrato Rodríguez [a], Luis Béjar Gómez [a]

[a] *Instituto de Investigaciones Metalúrgicas, UMSNH, Edificio U, Ciudad Universitaria. CP 58000, Morelia, Michoacán. México*
[b] *Instituto de Investigaciones en Materiales, UNAM, Ciudad Universitaria. Apartado Postal 70-360, 04510, México, DF. México*

Received 13 April 2006; accepted 21 June 2006

Abstract

Three Al–6Si–3Cu–*x*Mg alloys (x=0.59, 3.80 and 6.78 wt.%) were produced using melt-spinning. As-melt-spun ribbons were aged at 150, 180 and 210 °C for times between 0.05 and 100 h. Microstructural changes were examined using transmission electron microscopy (TEM) and microhardness was measured. TEM analysis of the as-melt-spun alloys revealed 5 nm nanoparticles and larger particles (50 nm) composed of Al_2Cu (θ) for the 0.59% Mg alloy and $Al_5Cu_2Mg_8Si_6$ (Q) for 3.80% and 6.78% Mg alloys. Silicon solid solubility was extended to 9.0 at.% and Mg in solid solution reached 6.7 at.%. After aging treatments the 6.78% Mg alloy exhibited the most significant increase in microhardness, reaching 260 kg/mm^2. TEM analysis of aged specimens also showed θ and Q phase (5–20 nm nanoparticles and 35–40 nm particles). The combination of the volume fraction and size of the particles plays an important role in microhardness variation.

Keywords: Melt-spun; Aluminum alloys; Magnesium; Aging; Recrystallization; Precipitation

1. Introduction

Among the aluminum alloys, the 319 series is one of the most widely used Al–Si–Cu alloys, particularly in the automotive industry. This alloy contains silicon and copper contents from 5.5 to 6.5 wt.% and from 3.0 to 4.0 wt.%, respectively. Magnesium is used for strengthening purposes at the expense of ductility. However, if the Mg content is lower than approximately 0.5 wt.%, no significant strengthening can be produced [1,2]. The main hardening constituent for the 319 alloy is Al_2Cu, which precipitates as nanosized particles after a T6 treatment. This treatment is particularly suitable for alloys with high Mg content in order to promote the formation of Mg_2Si. Al_2Cu and Mg_2Si are the main strengtheners in the peak aged condition [1]. For Al–Si–Cu–Mg alloys, precipitation of at least five different precipitates has been reported [3].

The Cu/Mg and Mg/Si ratios influence the nature of the various precipitates that form. A Cu/Mg ratio close to 2.0 (using at.%) leads to the preferential precipitation of Mg_2Si, while a ratio close to 8.0 promotes the formation of Al_2Cu [4]. A Mg/Si ratio lower than 8.0 promotes the formation of Al_2Cu, a ratio close to 3.0 promotes

* Corresponding author. Tel.: +52 443 3223500x 4009; fax: +52 443 322 3500x 4010.
E-mail address: post18@jupiter.umich.mx (I.A. López).

1044-5803/$ - see front matter © 2006 Elsevier Inc. All rights reserved.
doi:10.1016/j.matchar.2006.06.020

Table 1
Chemical composition (in wt.%) and Vickers microhardness of the experimental alloys

Alloy code	Si	Cu	Mg	Fe	Mn	Ti	Microhardness (kg/mm^2)
CAM01	6.40	3.02	0.59	0.34	0.09	0.14	164.33±4.25
CAM03	6.31	3.03	3.80	0.32	0.08	0.13	183.40±4.07
CAM06	5.84	2.95	6.78	0.31	0.07	0.12	181.65±5.20

Al_2CuMg, and Mg_2Si is favoured for ratios between 1.0 and 8.0 [5]. The cast structure for conventional Al–Si–Cu–Mg alloys includes α-Al, Si eutectic particles, Mg_2Si, Al_2Cu, $Al_5Cu_2Mg_8Si_6$ and other complex intermetallics [6], which results in low concentrations of alloying elements in solid solution even after the solution heat treatment. Thus, it is necessary to use a casting process that allows the attainment of a more supersaturated solid solution, avoiding or minimizing second phase formation.

The hypothesis of this work is that by applying a rapid solidification process (RSP), including melt-spinning, it is possible to retain higher quantities of alloying elements in solid solution and thereby modify the precipitation process. Parts produced by RSP could be used in engine cylinder sleeves, piston valve retainers, etc. [7]. RSP allows a reduction in grain size, extended solid solution ranges, reduced levels of segregation and, in some cases, the formation of metastable crystalline and amorphous phases [8,9]. The precipitation of a supersaturated solid solution in melt-spun alloys is usually accompanied by recrystallization, affecting the aged microstructures and the corresponding properties. The mutual actions between precipitation and recrystallization have been studied for steel, copper, nickel and aluminum based alloys [10–12]. Different explanations have been offered to infer the strengthening mechanism for RSP alloys. One argues that phases precipitate prior to recrystallization and impede the movement of dislocations, which then inhibit the recrystallization process. Another explains the favorable effect of recrystallization by the fact that recrystallization greatly refines the grain size and disperses the precipitates, resulting in higher microhardness after aging [12].

Previous work on the characterization of melt-spun Al–Si–Cu alloys [13] did not report the effects of RSP on structure and properties of the as-melt-spun and aged alloys when Mg is added. The first objective of this work is to discuss phase formation and microhardness relationships for three melt-spun ribbons with varying Mg contents. The second objective focuses on different

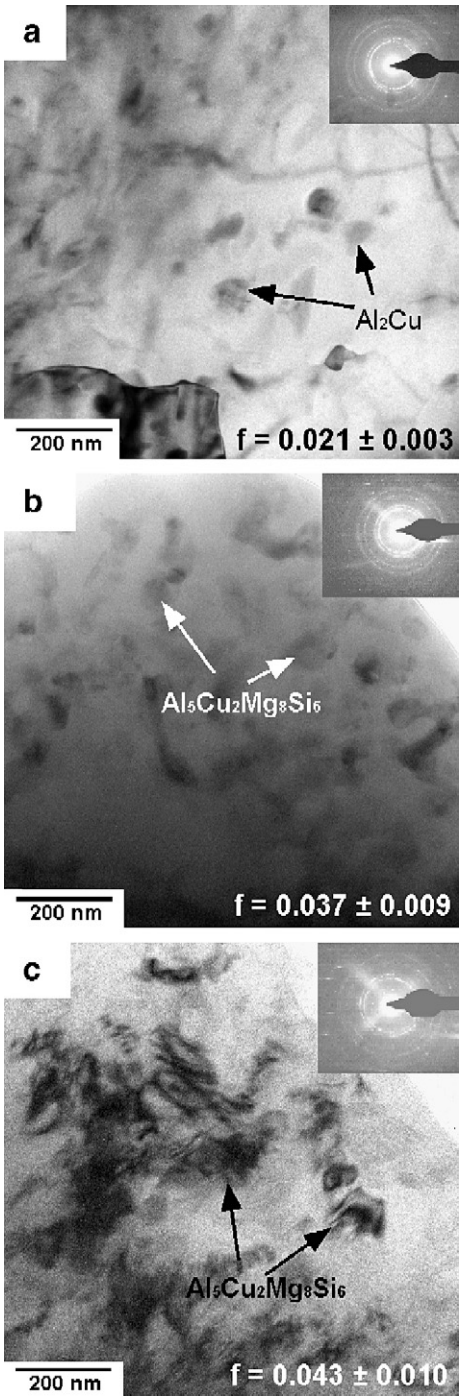

Fig. 1. Bright field transmission electron micrographs taken from the wheel side surface of the as-melt-spun ribbons for alloys with: (a) 0.59% Mg, (b) 3.80% Mg and (c) 6.78% Mg. Note Al_2Cu and $Al_5Cu_2Mg_8Si_6$ arrowed particles. The diffractions patterns represent the (111), (200), (220) and (311) reflection rings of the α-Al phase. Volume fraction of second phases (f) is shown.

aging treatment conditions and their effect on microstructure and microhardness.

2. Experimental

A 356 alloy ingot, with Al–8.5Si–0.3 Mg (wt.%), was used as raw material together with pure Cu (powder, >99.99% purity) and Mg (ingot, >99.95 % purity) to prepare alloys with three different Mg contents. Castings were carried out in an induction furnace under a controlled Ar atmosphere using graphite crucibles. Ingots were then remelted in a quartz tube and ejected through a 0.5-mm diameter aperture onto the surface of a 200-mm diameter polished copper wheel. The experiments were carried out under a helium atmosphere in order to avoid oxidation. The distance between the crucible orifice and the wheel was 7 mm. The ribbons were produced with a tangential speed of 30 m s^{-1}. The dimensions of the ribbons were 1–3 mm in width, 1–3 m in length and 20–60 μm in thickness. Experimental chemical compositions for the alloys prepared and their respective microhardness are given in Table 1.

As-melt-spun ribbon cross sections and chilling surfaces (in contact with the copper wheel) were characterized using transmission electron microscopy (TEM) and X-ray diffraction (XRD) techniques. XRD measurements were carried out in a Siemens 400 X-ray diffractometer using CuKα radiation at 30 kV and 25 mA. TEM investigations were done in a FEG-Philips Tecnai F20 operated at 200 kV. High resolution transmission electron microscopy (HRTEM) allowed observation of nanostructures. Specimens for TEM were prepared by dimpling in a Gatan 656 Dimple Grinder followed by Argon ion milling using a Gatan 691 Precision Ion Polishing System. Microhardness measurements were made with a Vickers diamond indenter in a Leitz Wetzlar microhardness tester employing a load of 25 g. Statistical procedures were carried out to ensure repetitive and accurate results.

As-melt-spun ribbons were aged at 150, 180 and 210 °C for times between 0.05 and 100 h and cooled in air. Assuming that the precipitation process must change the michorhardness even in the early stages of the process, the Vickers microhardness was measured and the influence of time and temperature on microhardness was plotted. Fine details of microstructure were revealed by TEM and related to the microhardness.

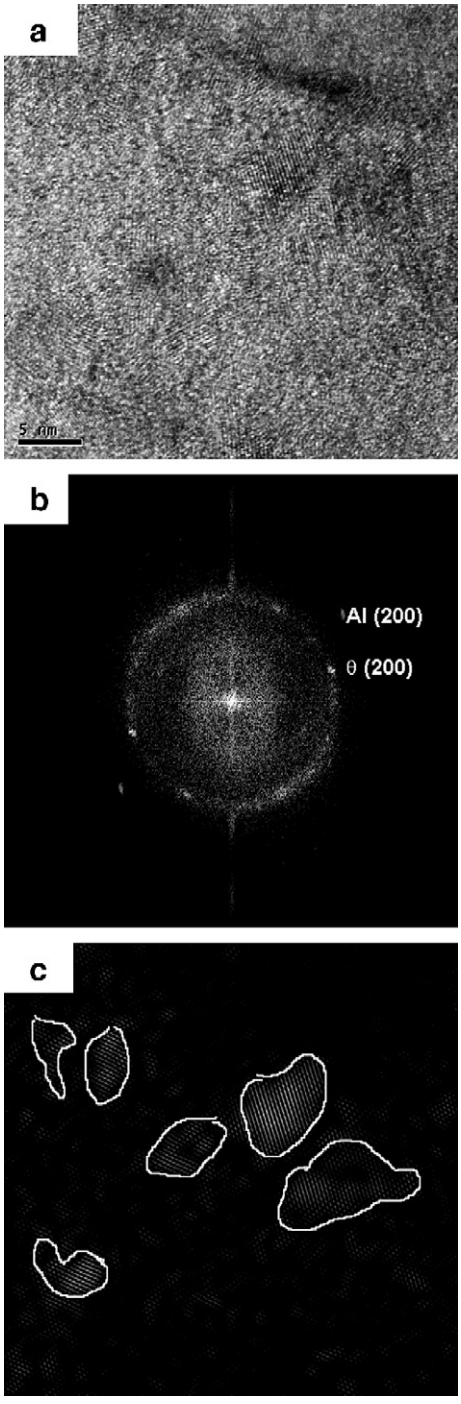

Fig. 2. (a) HRTEM micrograph for the 0.59% Mg ribbons, (b) FFT of the image and (c) filtered image showing Al_2Cu nanocrystallites.

Table 2
Chemical composition (in at.%), Cu/Mg and Mg/Si ratios in the supersaturated solid solutions for the experimental ribbons

Alloy code	Si	Cu	Mg	Cu/Mg ratio	Mg/Si ratio
CAM01	8.97	1.33	0.25	5.32	0.03
CAM03	6.60	1.01	2.55	0.40	0.39
CAM06	4.41	0.95	6.70	0.14	1.52

3. Results and discussion

3.1. Microstructure of as-melt-spun ribbons

Widespread solid solubility of alloying elements in the α-Al matrix as a consequence of rapid solidification has been reported extensively [7,9,10,11]. For the experimental alloys discussed here, total solubility was not found. TEM micrographs (Fig. 1a–c) show the presence of second phases of irregular shapes and sizes (approx. 50 nm). EDS analysis revealed that second phases correspond to Al_2Cu (θ) for the CAM01 (0.59% Mg) alloy and $Al_5Cu_2Mg_8Si_6$ (Q) for the alloys CAM03 (3.80% Mg) and CAM06 (6.78% Mg). By comparing the micrographs presented in Fig. 1a–c, it is observed that the increase in Mg content leads to a higher volume fraction (f) of second phases. The diffraction patterns inset in Fig. 1a–c show the characteristic interplanar distance rings of the α-Al phase. Reflection rings corresponding to the θ and Q phases are not observed, due to masking effects with α-Al interplanar distances. It was possible to significantly extend the solid solubility of Si in α-Al, reaching a maximum of 9 at.% for the CAM01 alloy, as is observed in Table 2. The increase in Mg content for the CAM03 and CAM06 alloys allowed the retention of higher concentrations of this element in the supersaturated solid solution compared to the CAM01 alloy, as can also be observed in Table 2. Mg is the main solid solution strengthener for Al alloys [1,2]. The increase in microhardness observed in Table 1 for the alloys CAM03 and CAM06 can be related to the higher quantity of alloying elements in solid solution (mainly Mg) and the presence of Q phase instead of θ. Cu/Mg ratios observed in Table 2 are markedly different from those obtained for conventionally cast alloys with the same chemical composition; this fact could modify kinetically and thermodynamically the precipitation process. In conventional 319 alloys Cu/Mg ratios are generally higher than 1.0, while for melt-spun alloys values as low as 0.14 were obtained (CAM06).

HRTEM was used to examine the nanostructure of the ribbons, characteristic of RSP alloys. As observed in Fig. 2a, Al_2Cu (θ) nanocrystallites are present in the α-Al matrix of the CAM01 alloy. The fast Fourier transform (FFT) showing the frequencies attributed to crystallites of

Table 3
Nanoparticles size and volume fraction

Alloy code	Volume fraction	Size (nm)
CAM01	0.048±0.002	3.87±0.91
CAM03	0.023±0.001	5.95±0.82
CAM06	0.015±0.0008	6.28±1.11

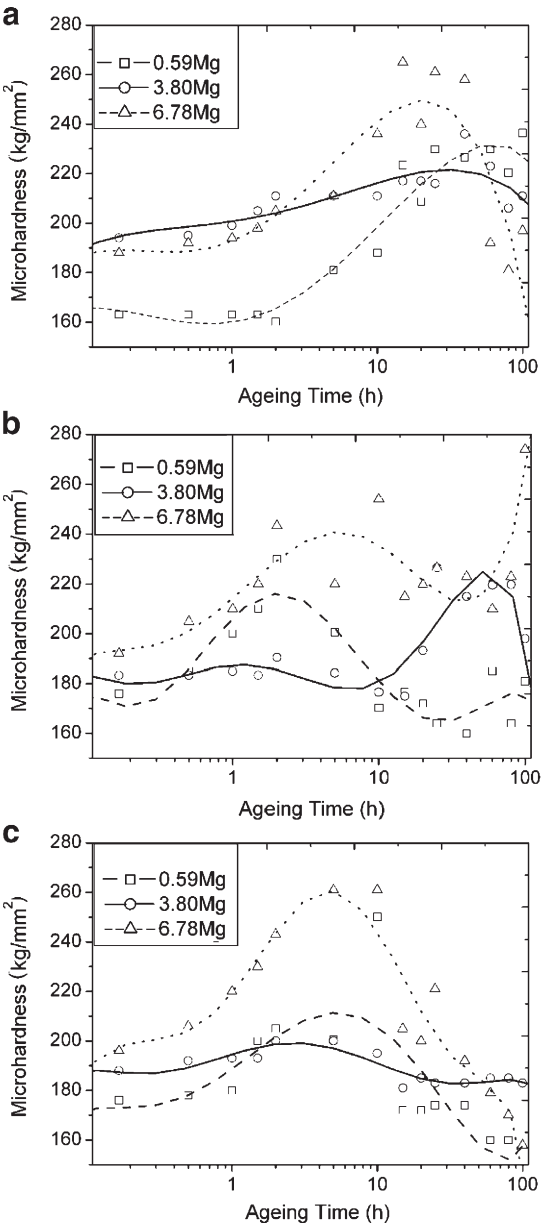

Fig. 3. Microhardness behaviour as a function of time and Mg content for the alloys aged at: (a) 150 °C, (b) 180 °C and (c) 210 °C. Note that the peak maximum shifts at shorter aging times as temperature increases.

θ and the α-Al phase is indexed in Fig. 2b. This fine structure (approx. 5 nm) which was not resolved by conventional TEM, was delineated by the IFFT image shown in Fig. 2c. Similar nanoparticles with chemical composition near to $Al_5Cu_2Mg_8Si_6$ (Q) were observed for CAM03 and CAM06 alloys. Orientation appears to be completely random, quite different from that for age-hardened Al alloys in which Guinier-Preston zones and

intermediate compounds precipitate on preferential crystallographic planes of the Al matrix [14]. It is worth noting that the interfaces between precipitates and the matrix are always incoherent. The size and volume fraction of the nanosized particles present in the as-melt-spun ribbons are indicated in Table 3. As shown in Table 3, the increase in Mg content leads to lower volume fraction and larger nanoparticle size.

3.2. Correlation between microstructure and microhardness

The microhardness behaviour for the aged ribbons as a function of aging times for different temperatures is shown in Fig. 3a–c. The most significant microhardness increase was obtained for the alloys with the highest Mg content (CAM06, 6.78% Mg), reaching 260 kg/mm^2. Maximum microhardness values for the alloys CAM01 (0.59% Mg) and CAM03 (3.80% Mg) are close to 220 kg/mm^2. Statistical analysis revealed that each of the three experimental parameters (aging time, aging temperature and Mg content) had significant effect on microhardness. The increase in Mg content from 0.59% to 6.78% leads to an increase in the microhardness values, and the microhardness is seen to vary inversely with aging time and temperature. High alloying element concentration in solid solution could explain the fact that small variations in experimental aging conditions give rise to significant changes in the precipitation response of the alloys due to the high driving force. This fact could lead to the formation of a higher volume fraction of precipitates with different chemical compositions and crystallographic structures. It is generally observed that, as the aging temperature increases, the maximum hardness peaks shift to shorter times, a fact that is generally observed in aged Al alloys and can be explained on the basis of diffusion rates.

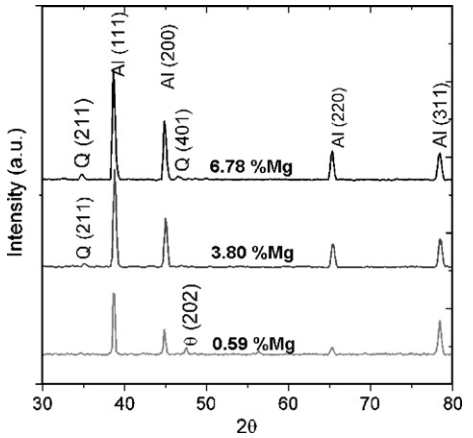

Fig. 4. XRD patterns for the experimental alloys aged at 180 °C in the peak aged conditions (2, 40 and 10 h for the alloys with 0.59%, 3.80% and 6.78% Mg, respectively).

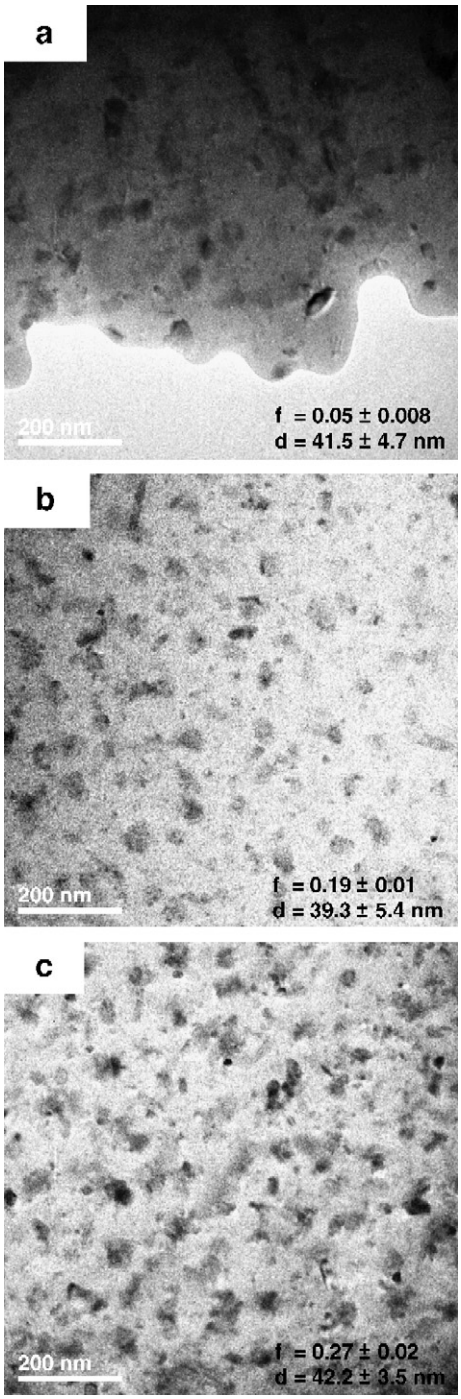

Fig. 5. TEM bright field micrographs showing the presence of Al_2Cu particles for the CAM01 alloy aged at 180 °C during: (a) 0.5 h, (b) 2 h (peak aged) and (c) 40 h (overaged). Particle size and volume fractions are shown.

XRD analysis, Fig. 4, shows that after aging a weak θ peak was discernable for CAM01 ribbons, while Q peaks are observed for CAM03 and CAM06 ribbons. These θ and Q phases were also observed in the as-melt-

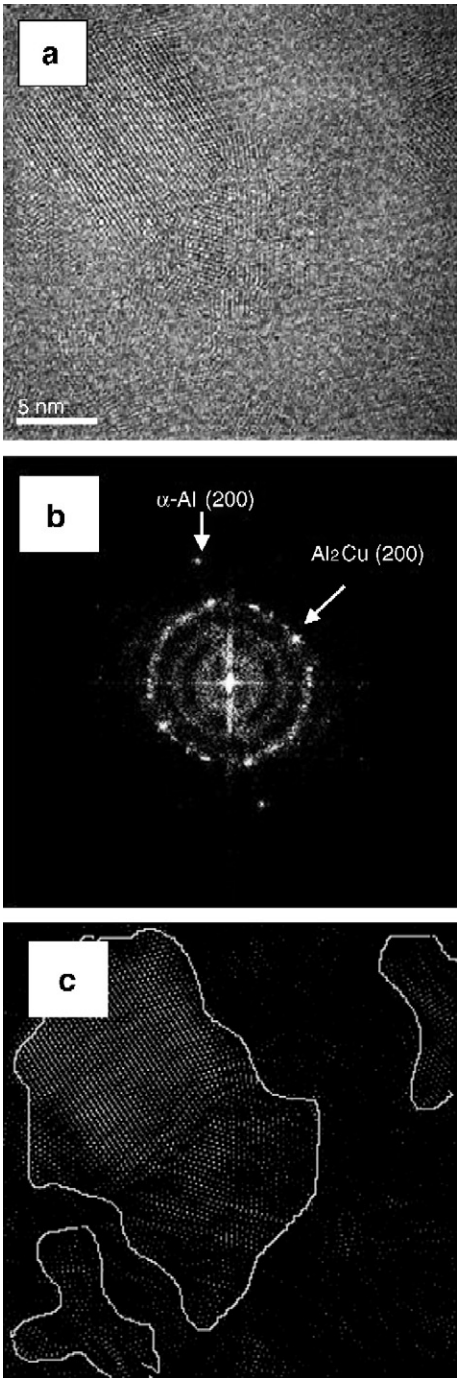

Fig. 6. (a) HRTEM image for the CAM01 alloy aged at 180 °C for 2 h (b) FFT showing the main frequencies for the matrix and the Al_2Cu particles and (c) Filtered image of the Al_2Cu particles.

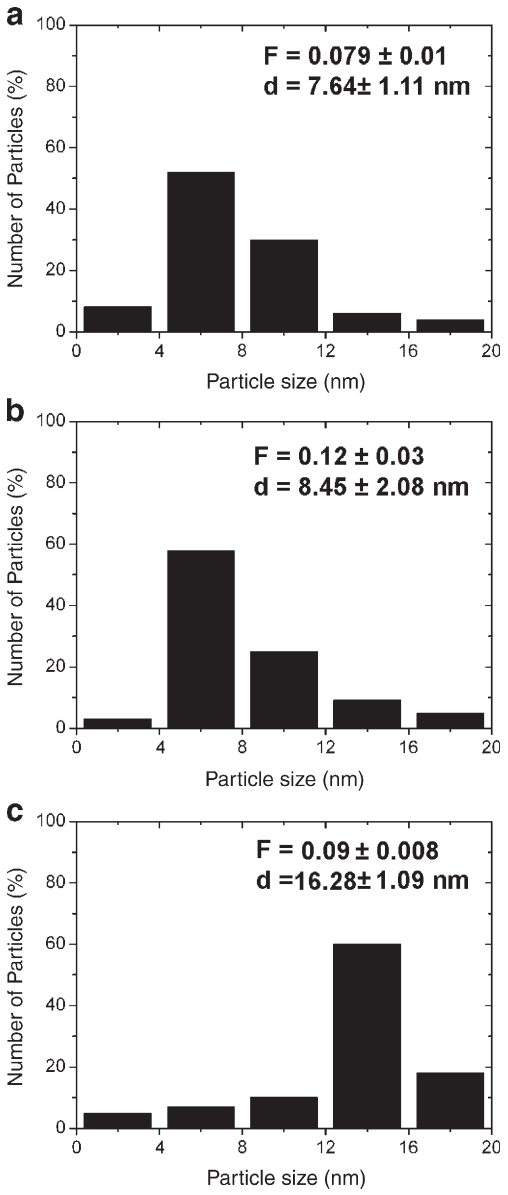

Fig. 7. Nanoparticle size distribution for the CAM01 alloy aged at 180 °C for: (a) 0.5 h, (b) 2 h and (c) 40 h. Average particle size and volume fraction are shown.

spun condition. The intensity of the Q peaks increase considerably for the alloy with higher Mg content. This means that the content of free Q phase is increased, an expected result due to the high quantity of Mg in solid solution in the CAM06 alloy.

3.2.1. Microstructure of aged 0.59% Mg Alloys

In order to explain the aging behaviour for the experimental alloys, the microstructural changes were analyzed by TEM. For the CAM01 alloy aged for 0.5 h at

180 °C (Fig. 5a), the microstructure is similar to that observed in the as-melted condition, containing a higher volume fraction (f=0.05) of precipitates, which leads to

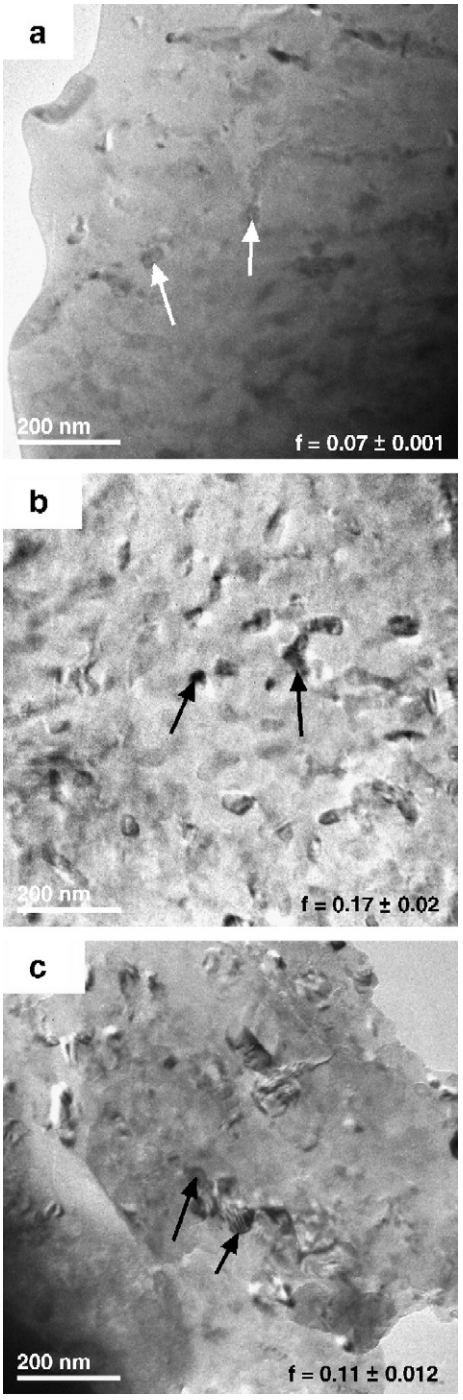

Fig. 8. TEM bright field micrographs showing the presence of Q precipitates (arrowed) with different volume fractions for the CAM03 alloy aged at 180 °C for: (a) 4 h, (b) 40 h (peak aged) and (c) 100 h (overaged). Volume fraction (f) is shown.

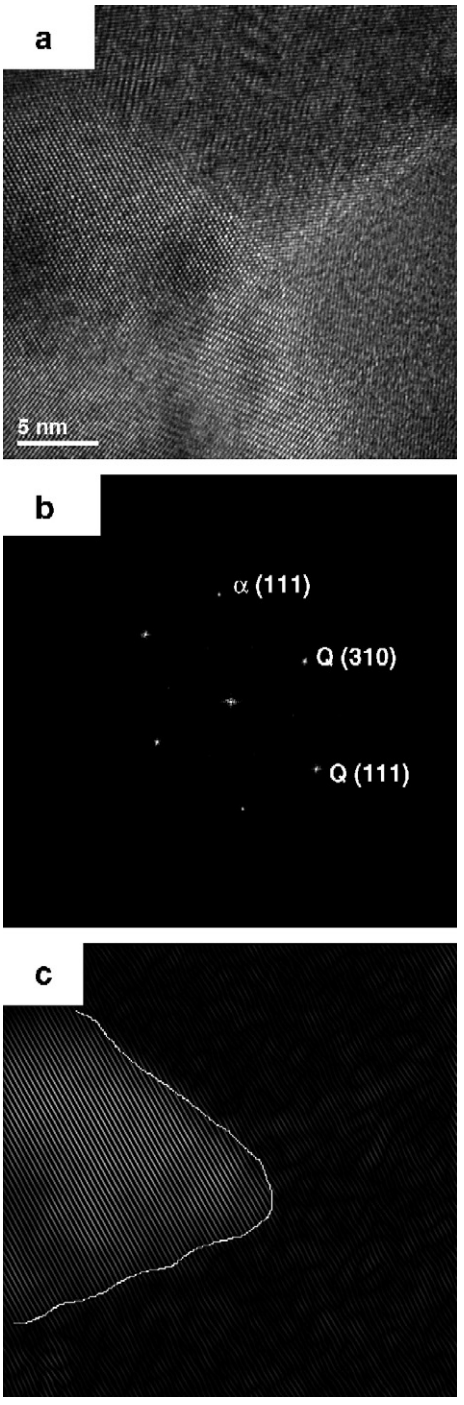

Fig. 9. (a) HRTEM image for the CAM03 alloy aged 2 h at 180 °C, (b) FFT showing the main frequencies for the matrix and the $Al_5Cu_2Mg_8Si_6$ particles and (c) filtered image of the $Al_5Cu_2Mg_8Si_6$ particles.

a microhardness increase. The EDS analysis revealed that the precipitates correspond to Al_2Cu, as might be anticipated for the supersaturated solid solution composition and the Cu/Mg ratio reported in Table 2. In the

peak 2-h aged condition (Fig. 5b), the precipitate volume fraction increases to 0.19, which is the main cause of the increase in microhardness, while the average particle size (d) remains approximately constant (Fig. 5a–c). After 40 h, an increase in the precipitate volume fraction can be observed, reaching 0.27 (Fig 5c). No other kind of precipitates was observed for any experimental condition, suggesting that Al_2Cu precipitates predominate and are responsible for the hardening properties.

In general, the strengthening behaviour due to nanosized particles with non-coherent interphases are

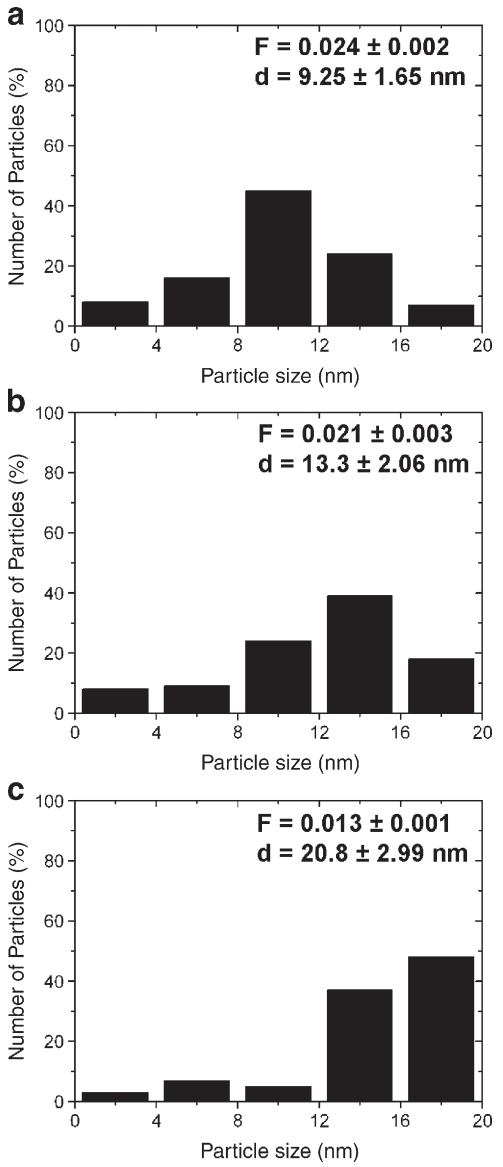

Fig. 10. Nanoparticle size distribution for the CAM03 alloy aged at 180 °C for: (a) 4 h, (b) 40 h and (c) 100 h. Average particle size and volume fraction are also shown.

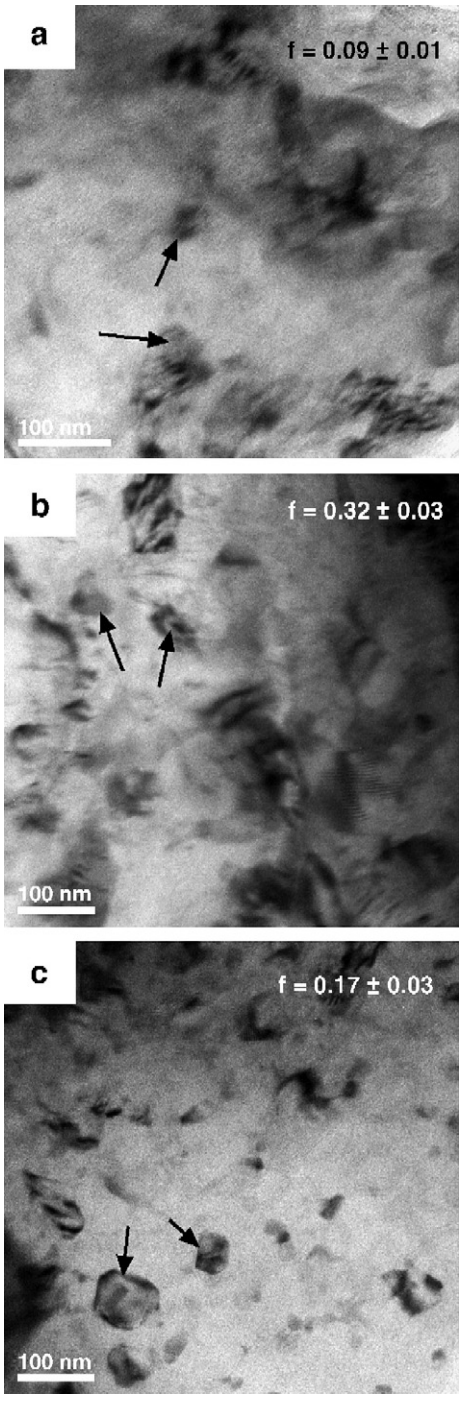

Fig. 11. TEM bright field showing the presence of Q precipitates (arrowed) for the CAM06 alloy aged at 180 °C for: (a) 2 h, (b) 10 h (peak aged) and (c) 60 h (overaged).

described by the Ashby-Orowan relationship [15], and can be given as

$$\Delta\sigma = (0.538Gbf^{1/2}/d)\ln(d/2b) \quad (1)$$

Where $\Delta\sigma_y$ is the increase in yield strength (MPa), G is the shear modulus (MPa), b is the Burgers vector (mm), f is the volume fraction of the particles and d is the diameter of the particles (mm). Eq. (1) predicts that a higher volume fraction of precipitates leads to alloy strengthening, while the dominant effect of the reciprocal of particle diameter over the logarithmic term indicates that strengthening decreases for larger particles. In addition to the 40-nm diameter Al_2Cu particles observed in Fig. 5a–c for the CAM01 alloy, HRTEM showed crystalline domains present in nanosized Al_2Cu particles, as shown in Fig. 6a for the peak aged condition (2 h). The corresponding fast Fourier transform (FFT) observed in Fig. 6b shows the most important frequencies, while the filtered image for the (200) plane in Fig. 6c shows the interplanar distance corresponding to Al_2Cu (3.04 Å). These nanoparticles were observed for all aging conditions and their formation is attributed to the recrystallization process. Particles with coherent interfaces were not observed.

The quantitative analysis of the nanosized Al_2Cu particles revealed that the particle size increased with time, while the volume fraction does not show a consistent trend; this can be seen in the histograms in Fig. 7a–c. Maximum strengthening is obtained for a critical combination of particle size and volume fraction for particles and nanoparticles, as implied by Eq. (1). The presence of two kinds of particles, with different sizes, that play a significant role in the peak aged microhardness condition, complicates the interpretation of the phenomena. If only the terms involving d and f in Eq. (1) are taken into account, $\Delta\sigma_y$ is:

$$\Delta\sigma_y \sim \left(\frac{f^{1/2}}{d}\right)\ln d \tag{2}$$

The contributions in Eq. (2) to $\Delta\sigma_y$ by the particles ($\Delta\sigma_{yp}$) and the nanoparticles ($\Delta\sigma_{yn}$) can be calculated as follows:

$$\Delta\sigma_y = \Delta\sigma_{yp} + \Delta\sigma_{yn} \tag{3}$$

Calculating $\Delta\sigma_y$ for the experimental conditions (d in nm), it was found that the maximum value (0.13) occurs for the peak aged condition, while lower $\Delta\sigma_y$ values were obtained for the initial strengthening and the overaged condition (0.09).

3.2.2. Microstructure of aged 3.80% Mg alloys

The microstructural changes after aging for the alloy with 3.80% Mg (CAM03) at 180 °C can be observed in Fig. 8a–c. As can be observed in Fig. 8a, the structure after 4 h is similar to that observed in the as-melt-spun condition (see Fig. 1b), with the presence of irregular Q phase. An increase in the Q phase volume fraction to 0.17 is observed in the peak aged condition (40 h), Fig. 8b; this is considered to be the main cause for the increase in microhardness. The decrease in the Q phase volume fraction after 100 h, Fig. 8c (overaged condition), results in a decrease in microhardness values.

Nanosized particles were also observed for CAM03 alloys aged at 180 °C. The presence of $Al_5Cu_2Mg_8Si_6$ crystalline domain nanoparticles for specimens aged for 2 h is observed in HRTEM in Fig. 9a. The corresponding FFT in Fig. 9b shows the most important frequencies, while the filtered image for the (200) plane in Fig. 9c shows the 3.16 Å interplanar distance of the $Al_5Cu_2Mg_8Si_6$ phase. Particles with coherent interfaces were not observed.

Quantitative image analysis of the nanosized $Al_5Cu_2Mg_8Si_6$ particles in CAM03 revealed that particle size increases with time, whereas the volume fraction decreases, as can be observed in Fig. 10a–c. This fact is also related to the maximum microhardness for a critical particle size and volume fraction and is attributed to recrystallization and Ostwald ripening processes. The maximum $\Delta\sigma_y$ (0.07) was calculated for the peak aged (40 h) condition; this decreased to 0.05 in the overaged condition.

3.2.3. Microstructure of aged 6.78% Mg alloys

The phase distribution and morphology changes after different aging times for the alloy with 6.78% Mg (CAM06) aged at 180 °C can be observed in Fig. 11a–c. After 2 h (Fig. 11a), the microstructure resembles the as-melt-spun condition (see Fig. 1c), with irregular phases corresponding to Q. After 10 h, the peak aged condition (Fig. 11b), the particles tend to more regular interfaces, with a higher volume fraction (0.32) and an average particle size of 34.0 nm. After overaging for 60 h, particle coarsening occurs, reaching 43.3 nm (Fig 11c) and resulting in a reduction of precipitate volume fraction to 0.17. The presence of nanoparticles for this aged alloy and the behaviour of measured $\Delta\sigma_y$ agrees with the microhardness trend.

4. Conclusions

The effect of magnesium content and thermal aging heat treatments on the microstructure of three quaternary Al–Si–Cu–Mg melt-spun alloys containing 0.59, 3.80 and 6.78 wt.% Mg were studied. From the analysis of the results, the following conclusions can be drawn:

1. TEM analysis revealed the presence of irregularly shaped approximately 5 nm nanoparticles and particles with larger size (approximately 50 nm) in the as-melt-

spun alloys. An increase in the Mg content leads to a higher second phase volume fraction that initiates an increase in microhardness. Chemical composition of second phases corresponded to Al_2Cu (θ) for the alloy with 0.59% Mg and $Al_5Cu_2Mg_8Si_6$ (Q) for the alloys with 3.80% and 6.78% Mg.

2. A maximum solid solubility value of 9.0 at.% for Si in α-Al was obtained for the as-melt-spun alloys. The increase in the Mg content for the Al–6Si–3Cu–*x*Mg alloy showed that the quantity of Mg in solid solution increased from 0.25 at.% to 6.7 at.%. This increase in microhardness is also related to the higher concentration of alloying elements in solid solution.
3. Aging heat treatments significantly enhance microhardness values for melt-spun alloys, reaching approximately 50% higher values. After aging, the alloy with 6.78% Mg (CAM06) exhibited the most significant increase in microhardness, reaching 260 kg/mm^2, which emphasizes the importance of the increase in Mg content. Microhardness values for the alloys with 0.59% and 3.80% Mg were close to 220 kg/mm^2. The highest microhardness is related to a high concentration of alloying elements in solid solution, which initiate a more substantial precipitation response. Generally, increasing aging temperature decreases microhardness and shifts the maximum peak to shorter aging times.
4. Chemical composition of the precipitates is similar to the particles present in the as-melt-spun condition, corresponding to Al_2Cu (θ) for the alloy with 0.59% Mg and $Al_5Cu_2Mg_8Si_6$ (Q) for the alloys with 3.80% and 6.78% Mg. No other precipitates were observed.
5. The microstructure of the aged alloys consists of nanoparticles (5–20 nm) obtained by recrystallization, and larger particles (approximately 40 nm) formed by the Ostwald ripening process. Microhardness values depend on the combination of volume fraction and particle size for the two kinds of particles, exhibiting peak aging effects at critical concentrations.

Acknowledgements

The authors would like to thank F. Solorio, G. Lara and R.D. Cervantes for technical assistance, and they also acknowledge the financial support provided by CIC and CGEP (UMSNH), México, and the material provided by Castech S.A. de C.V.

References

[1] Ouellet P, Samuel FH. Effect of Mg on the aging behaviour of Al–Si–Cu 319 type aluminium casting alloys. J Mater Sci 1999;34:4671–97.
[2] Samuel FH, Samuel AM, Liu H. Effect of magnesium content on the ageing behaviour of water chilled Al–Si–Cu–Mg–Fe–Mn (380) alloy casting. J Mater Sci 1995;30:2531–40.
[3] Yao J, Edwards GE, Graham DA. Precipitation and age-hardening in Al–Si–Cu–Mg–Fe casting alloys. Mater Sci Forum 1996;217–222:777–82.
[4] Gomes RM, Sato T, Tezuka H. Precipitation strengthening and mechanical properties of hypereutectic P/M Al–Si–Cu–Mg alloys containing Fe and Ni. Mater Sci Forum 1996;217–222:789–94.
[5] Murayama M, Hono K, Saga M, Kikushi M. Atom probe studies on the early stages of precipitation in Al–Mg–Si alloys. Mater Sci Eng A 1998;250:127–32.
[6] Li Z, Samuel AM, Samuel FH, Ravindran C, Valtierra S. Effect of alloying elements on the segregation and dissolution of Al_2Cu phase in Al–Si–Cu 319 alloys. J Mater Sci 2003;38:1203–18.
[7] Reyburn B, Corbin S, Hunt WH. New directions in aluminum-based P/M materials for automotive applications. Int J Powder Metall 2000;36:59.
[8] Wesseling P, Ko BC, Lewandowski JJ. Quantitative evaluation of a-Al nano-particles in amorphous $Al_{87}Ni_7Gd_6$ comparison of XRD, DSC, and TEM. Scr Mater 2003;48:1537–41.
[9] Liebermann HH. Rapidly solidified alloys made by chill block melt-spinning processes. J Cryst Growth 1984;70:497–506.
[10] Liu P, Kang BX, Cao XG, Huang JL, Yen B, Gu HC. Aging precipitation and recrystallization of rapidly solidified Cu–Cr–Zr–Mg alloy. Mater Sci Eng A 1999;265:262–7.
[11] Kusy M, Riello P, Battezzati L. A comparative study of primary Al precipitation in amorphous Al87Ni7La5Zr by means of WAXS, SAXS, TEM and DSC techniques. Acta Mater 2004;52:5031–41.
[12] Pons J, Segui C, Chernenko VA, Cesari E, Ochin P, Portier R. Transformation and ageing behaviour of melt-spun Ni–Mn–Ga shape memory alloys. Mater Sci Eng A 1999;273:315–9.
[13] Lutfi M, Unlu NP, Eruslu N, Genc E. Characterization investigations of a melt-spun ternary Al–8Si–5.1Cu (in wt.%) alloy. Mater Lett 2003;57:3296–301.
[14] Inoue A. Amorphous, nanoquasicrystalline and nanocrystalline alloys in Al-based systems. Mater Lett 1997;31:87–92.
[15] Gladman T. Precipitation hardening in metals. Mater Sci Technol 1999;5:30–6.